



Empirical prediction for travel distance of channelized rock avalanches in the Wenchuan earthquake area

Weiwei Zhan, Xuanmei Fan, Runqiu Huang, Xiangjun Pei, Qiang Xu, Weile Li

State Key Laboratory of Geohazard Prevention and Geoenvironment Protection, Chengdu University of Technology, Chengdu, 610059, China

Correspondence to: Xuanmei Fan (fxm_cdut@qq.com)

Abstract. Rock avalanches are extremely rapid, massive flow-like movements of fragmented rock. The travel path of the rock avalanches may be confined by channels in some cases, which were named as the channelized rock avalanches. Channelized rock avalanches are potentially dangerous due to their hardly predictable travel distance. In this study, we constructed a dataset with detailed characteristic parameters of 38 channelized rock avalanches triggered by the 2008 Wenchuan earthquake using the visual interpretation of remote sensing imagery, field investigation, and literature review. Based on this dataset, we assessed the influence of different factors on the runout distance and developed prediction models of the channelized rock avalanches using the multivariate regression method. The results suggested that the movement of channelized rock avalanche was dominated by the landslide volume, total relief, and channel gradient. The performance of both models was then tested with an independent validation dataset of 8 rock avalanches that induced by the 2008 Wenchuan, the Ms7.0 Lushan earthquake, and heavy rainfall in 2013, showing acceptable good prediction results. Therefore, the travel distance prediction models for channelized rock avalanches constructed in this study is applicable and reliable for predicting the run out of similar rock avalanches in other regions.



Keywords: channelized rock avalanches; travel distance; empirical prediction; multivariate regression model; Wenchuan earthquake

1 Introduction

Rock avalanches are extremely rapid, massive flow-like movements of fragmented rock from a very large rock slide or rock fall (Hogg et al. 2014). Hundreds of rapid and long run-out rock avalanches were triggered by 2008 Wenchuan earthquake in Sichuan Province (Zhang et al. 2013), with



30 catastrophic consequences for residents in the affected areas. For instance, the $1.5 \times 10^7 \text{ m}^3$ Donghekou
 31 rock avalanche in Qingchuan County, near the seismogenic fault, traveled 2.4 km, killing about 780
 32 persons and destroying four villages (Zhang et al. 2013). Rock avalanches can cause incredible damage
 33 due to their characteristics of high-speed and unexpectedly long runout, while their transport
 34 mechanisms are still considered to be controversial among many researchers (Hungr et al. 2001).
 35 Therefore, constructing prediction models for rock-avalanche travel distance is meaningful in terms of
 36 not only theoretical research on motion mechanisms but also in practical application for mitigation of
 37 rock-avalanche risk.

38 Methods for determining the travel distance of landslides can be divided into two categories: dynamic
 39 modeling (Heim 1932; Hungr et al. 2009; Lo et al. 2011; Pastor et al. 2009; Sassa 1988), and empirical
 40 modeling (Scheidegger 1973; Lied et al 1980; Finlay et al. 1999; W  et al. 2006; Guo et al. 2014).
 41 The dynamic models provide information on landslide intensity, such as velocity, affected area and
 42 deposition depth, in addition to travel distance. Nonetheless, dynamic models require accurately
 43 quantified input parameters that are difficult to obtain before the events, and many simplified
 44 assumptions that are not applicable to the actual situation. Empirical models considering the
 45 correlations between observational data provide an effective technique to aid in understanding
 46 mechanisms of rock-avalanche motion and to develop practical models for predicting rock-avalanche
 47 travel distance. However, the empirical-statistical models set up from samples with different
 48 geomorphological and geological surroundings, trigger conditions, or failure modes are not very
 49 sufficient to be applied to Wenchuan earthquake area .

50 In this study, we compiled a dataset of 38 rock avalanches with flow paths confined by channels (this
 51 kind of landslide is hereinafter termed as channelized rock avalanche) from interpretation of remote
 52 sensing, field investigations and literature review (see Section 3.1). Statistical correlations were used to
 53 determine the principle factors affecting the mobility of the channelized rock avalanches. Then a
 54 stepwise multivariate regression model was developed to build a best-fit empirical model for the travel-
 55 distance prediction of this kind of rock avalanches in the Wenchuan earthquake area. A derivative
 56 multivariate regression model was also constructed. The performance of both models was then tested
 57 with an independent validation dataset of 8 rock avalanches in the same area.

58



59 2 Rock avalanches in study area

60 The study area (see Figure 1) is on the northeast-trending Longmenshan thrust fault zone between the
 61 Sichuan basin and the Tibetan plateau. Three major sub-parallel faults are: the Wenchuan-Maowen
 62 fault, the Yingxiu-Beichuan fault and the Pengguan fault (Fan et al., 2014). With highly developed
 63 stream systems, this region is characterized by high mountains and deep valleys and extreme rates of
 64 erosion (Fu et al 2009; Qi et al 2011).

65 This study selected 38 channelized rock avalanches induced by the Wenchuan earthquake to study the
 66 relations between travel distance and influential factors. These rock avalanches occurred along the
 67 seismogenic Yingxiu-Beichuan fault; the distance to the fault ranged from 0 m ~21,300 m with a mean
 68 value of 3,895 m. Another distribution characteristic was that these rock avalanches mainly clustered
 69 on the step-overs, bends and distal ends of the seismogenic fault. These distribution characteristics of
 70 the large rock avalanches suggested that the occurrence of rock avalanches was associated with very
 71 strong earthquake ground motion. The Wolong Station recorded the highest seismic acceleration with
 72 the peak ground acceleration reaching 0.948g vertically and 0.958g horizontally (Yu et al., 2009).
 73 Locally, the ground motion was high enough to throw rocks into the air.

74 The lithology of outcropping rock in source areas can be divided to four types: carbonate rock, phyllite,
 75 igneous rock and sandstone. The landslide deposit of the rock avalanches in the study area structure
 76 was usually debris, which suggests that the sliding masses were intensively fragmented during their
 77 movement.

78 The influence of the local geomorphology on the paths of the rock avalanches was obtained from
 79 remote-sensing images after the events. Although the rock avalanches we chose all had flow paths
 80 confined by channels, some topographic differences were found to be significant in affecting present
 81 that had affected the shape morphology of the rock avalanche deposits. The source areas had well-
 82 defined boundaries. When the source mass was detached from the slide bedrock, it may directly
 83 move into the channel down slope (see Figure 2b), or access the channel with enter it at some impact
 84 transition angle of movement direction (see Figure 2a). The channel itself may have changes in
 85 direction and inclination. The distal end of the landslide may lie stop in the channel (see Figure 2a) or
 86 may reach the valley or plain (see Figure 2b).

87



88 The study area (see Figure 1) is on the northeast-trending Longmenshan thrust fault zone between the
 89 Sichuan basin and the Tibetan plateau. Three major sub-parallel faults are: the Wenchuan-Maowen
 90 fault, the Yingxiu-Beichuan fault and the Pengguan fault (Wang et al., 2014). With highly developed
 91 stream systems, this region is characterized by high mountains and deep valleys and extreme rates of
 92 erosion (Fu et al 2009; Qi et al 2011).

93 This study selected 38 channelized rock avalanches induced by the Wenchuan earthquake to study the
 94 relations between travel distance and influential factors. These rock avalanches occurred along the
 95 seismogenic Yingxiu-Beichuan fault; the distance to the fault ranged from 0 m ~21,300 m with a mean
 96 value of 3,895 m. Another distribution characteristic is that these rock avalanches mainly clustered on
 97 the step-overs, bends and distal ends of the seismogenic fault. These distribution characteristics of the
 98 large rock avalanches suggested that the occurrence of rock avalanches was associated with very strong
 99 earthquake ground motion. The Wolong Station recorded the highest seismic acceleration with the peak
 100 ground acceleration reaching 0.948g vertically and 0.958g horizontally (Yu et al., 2009). Locally, the
 101 ground motion was high enough to throw rocks into the air.

102 The lithology of outcropping rock in source areas can be divided to four types: carbonate rock, phyllite,
 103 igneous rock and sandstone. The deposit of the rock avalanches in the study area is usually debris,
 104 which suggests that the sliding masses were intensively fragmented during their movement.



105 The influence of the local geomorphology on the paths of the rock avalanches was obtained from
 106 remote-sensing images after the events. Although the rock avalanches we chose all had flow paths
 107 confined by channels, some topographic differences were found to be significant in affecting the
 108 morphology of the rock avalanche deposits. When the source mass was detached from the bedrock, it
 109 may directly move into the channel down slope (see Figure 2b), or enter the channel with some
 110 transition angle of movement direction (see Figure 2a). The channel itself may have changes in
 111 direction and inclination. The distal end of the landslide may stop in the channel (see Figure 2a) or may
 112 reach to wide valley or plain (see Figure 2b).

113




114 3 Data and method

115 3.1 General consideration

116 Various statistical methods have been applied to predict travel distance of landslides. The most
 117 prevalent one is the equivalent friction coefficient model, which only takes account of landslide volume
 118 (Scheidegger 1973). Another well-known model is the statistical α - β model in which the maximum
 119 runout distance is solely a function of geography  et al., 1980; Gauer et al., 2010). Finlay et
 120 al.(1999) developed some multiple regression models containing slope geometric parameters like slope
 121 height and slope angle for the travel distance prediction of landslides on the artificial slopes upon the
 122 horizontal surface. Based on the data of 54 landslides which was relatively open or confined by gentle
 123 lateral slope, Guo et al.(2014) established an empirical model for predicting landslide travel distance in
 124 Wenchuan earthquake area and suggested that rock type, landslide volume, and slope transition angle
 125 play dominant roles on landslide travel distance. And there are increasing sound that the prediction
 126 models of travel distance should adapt to different types of landslides (Corominas 1996; Fan et al,
 127 2014;). 

128 Moreover, the local morphology plays an important role on shape and mobility of rock avalanches.
 129 Heim (1932) firstly mentioned the influence of local morphology that the debris masses will undergo
 130 different effects with the angle of impact changing, and rock avalanches has to conform to the local
 131 morphology regardless of their scale. Abele (1974) summarized four different possibilities of
 132 adaptation of the rock avalanche to local morphology. Hsu(1975) noted that a sinuous pathway can
 133 reduced runout distance of rock avalanches. Nicoletti (1991) inferred that local morphology impacts on
 134 landslide motion through changing the rate of total energy dissipation along the travel path. To
 135 determine the influence of specific channels on the travel distances of rock avalanches, we respectively
 136 consider the impacts of gradients of the upper slopes and lower channels.

137 Rock avalanches triggered by Wenchuan earthquake usually initiated from top or the higher part of
 138 slopes possibly due to the altitude amplification effect of earthquake acceleration, therefore the toe of 
 139 the rupture surface were commonly found in the source area at the upstream of the channel (See Figure
 140 3). When the slope failed, the failed mass travelled a long distance down the channel. The 38 rock
 141 avalanches in this study are selected with the criterion that the flow path is partially or fully confined
 142 by channels. The volumes of these rock avalanches ranged from $0.4\text{--}50 \times 10^6 \text{m}^3$; with horizontal travel



143 distances between 0.58 and 4.00 km. The volume is prior to the area to be put into the travel distance
 144 prediction model as it had much more physical meanings. And we introduced total relief as well as the
 145 height of source area to probe the influences of the potential energy difference and altitude difference
 146 of source mass on the travel distance of the rock avalanches.

147 3.2 Data

148 The terms and notations of a typical channelized rock avalanche are shown in Figure 3. The local
 149 morphology of a rock avalanche can be divided to three sections: initiated slope (source area), channel
 150 (main travel path or flow area) and valley floor (deposition area). When the mass moves over the slope
 151 section, it is free from lateral constraints, and the moving mass is able to spread laterally. After entering
 152 the channel, the flowing mass is constrained by the two lateral slopes. Finally, the mass may reach to a
 153 wide valley floor, where it spreads laterally and deposits. The average inclination of slope section and
 154 valley section are obtained respectively, while the gradient of valley section is neglected as it has very
 155 little variation. Slope angle (α), denotes the average inclination of the initiated slope section.
 156 Channel angle (β), denotes the average inclination of the sectional channel. Source area height (Hs),
 157 denotes the elevation difference between the crest of the sliding source and the toe of the rupture
 158 surface. Total relief (H) is the elevation difference between the crest of the sliding source and the distal
 159 end of the debris deposit. Travel distance (L) is the horizontal distance between the crest of the sliding
 160 source and the distal end of the debris deposit. Landslide area (A) is the source area of the rock
 161 avalanche obtained from remote sensing image interpretation. An empirical scaling relationship with
 162 different empirical coefficients is frequently used to link the volume and the area of landslides in
 163 different areas or with different types, and we chose the one developed by Parker et al. (2011) in the
 164 same study area. Some of some rock avalanches with detailed field investigation are replaced by the
 165 data from published literature. The parameters of 38 rock avalanches are listed in Table 1.

166 3.3 Method

167 Travel distance is the most desirous prediction in rock-avalanche hazard evaluation in mountainous
 168 areas. Travel distance prediction of rock avalanche is a complicated issue as it is determined by many
 169 different properties of the materials (i.e., grain size distribution and water content), topographical
 170 factors, mobility mechanics of failed mass, the confinement attributes of travel path, and so on (Guo et



al., 2014). Empirical-statistical methods have long been used as tools to study the mobility of rock avalanche since they are easy to develop and apply, and they are not dependent on knowing the physical processes involved in causing the mobilized channelized rock avalanches have unique movement paths involving complex, and possibly little-known physical processes such as grain collisions, fragmentation and entrainment of bed material from the channel sides and bottom. Existing empirical models have not produced a favourable prediction. The forecasting index system and the prediction model of channelized rock avalanches should be discussed first.

In this paper, we first selected controlling factors on rock avalanche travel distance through correlation analysis. Then we fitted a stepwise multivariate regression model using all significant correlation variables to obtain a best-fit empirical model for landslide travel distance, and explored which factors were statistically significant at the same time, as expressed in equation (1).

$$y = b_0 + b_1x_1 + b_2x_2 + b_3x_3 + \dots + b_nx_n + \varepsilon \quad (1)$$

where y is the predictant ('dependent variable'), e.g. travel distance of rock avalanche ($i = 1, 2, \dots, n$) are the predictors ('independent variables'), b_0 is the intercept, b_i ($i = 1, 2, \dots, n$) are the regression coefficients of the corresponding x_i , and ε is the residual error, here assumed to be independently and normally distributed. Predictors were added to the regression equation one at a time until there was no significant improvement in parsimonious fit as determined by the adjusted R^2 .

4 Results and validation

4.1 Relationships between travel distance and volume, topographic relief of rock avalanche

Correlation coefficients between different variables and travel distance (L) were calculated first, generating the correlation coefficients matrix shown in Table 2. The significant relevant predictors with the 95% confidence for travel distance prediction of channelized rock avalanche are landslide area (A), landslide volume (V), total relief (H_t), source area height (H_s), and channel angle (β), with correlation coefficient of 0.877, 0.866, 0.857, 0.675, -0.467, respectively.

Figure 4 illustrates that the travel distance (L) varies exponentially with volume (V) of rock avalanche with an exponential exponent of 0.377. Compared with a compilation of world-wide rock-avalanche data (Legros, 2002), the mobility of rock avalanches in our study area is stronger than other non-volcanic landslides (power exponent 0.25), but weaker than volcanic landslides and debris flows



(both power exponent is 0.39). The relation between travel distance (L) and total relief (H) is shown in figure 5. The result suggests that the mobility (travel distance) of rock avalanche has relatively strong linear relationship with total relief (H). The scale factor is close to 2.4, which means that the apparent friction coefficient (H/L) for the rock avalanches is approximately 0.42. This is significantly lower than the commonly observed static coefficient of friction of rock material (~ 0.6).

4.2 Multivariate regression model of rock avalanche travel distance

According to the matrix of correlation coefficients (Table 2), the slope angle (α) does not have a significant correlation with travel distance (L) at the 95% confidence level. Thus this variable could be excluded first during development of the best-fit regression model for travel distance prediction. Prior to the landslide area (A), the landslide volume (V) has been considered in the models as it has much more physical meaning. In the end, a stepwise linear multivariate regression technique was applied to find the best-fit travel distance regression model using the significant relevant predictors including landslide volume (V), total relief (H), source area height (H_s) and channel angle (β). The best-fit regression equation for travel distance prediction were derived from the dataset of Table 1 (see equation (2)), and the coefficient of the variables with 95% confidence are shown in Table 3.

$$\log(L) = 0.420 + 0.079 \log(V) + 0.718 \log(H) - 0.361 \log(\tan \beta) \quad (2)$$

Where \log is the logarithm of 10; L is the predicted travel distance (m); V is the landslide volume (m^3); H is the total relief (m); β is the mean gradient of the channel ($^\circ$).

Equation (2) can be transformed to equation (3):

$$L = 2.630 V^{0.079} H^{0.718} (\tan \beta)^{-0.365}$$

The best-fit travel distance regression equation indicates that the travel distance of channelized rock avalanche is positively correlated with landslide scale (landslide volume) and potential energy loss (total relief), and negatively correlated with channel gradient (channel angle), which is coherent with the results of correlation analysis in table 2.

While the total relief (H) will be unknown prior to landslide occurrence, the elevation difference of source area will be available through specific field investigation on a potential rock avalanche area.

Hence, we introduced H_s and α in replacement of H to the regression model as they have relative high correlation with H (correlation coefficients are 0.801 and 0.49 respectively). The transformed



alternative regression equation is given as equation (4) with the coefficient of the variables with 95% confidence in table 3.

$$L = 3.6V^{0.303}H_s^{0.244}(\tan \alpha)^{-0.115}(\beta)^{0.072} \quad (4)$$

Where L is the predicted travel distance (m); V is the landslide volume (m³); H_s is the height of source area (m); α is the mean angle of slope segment (°); β is the mean gradient of the channel segment (°).

The validity of these two models were evaluated through the significance test leading to the highest R² value and the lowest residual standard error. Table 3 shows the significance values for the prediction model equations. Adjusted R² means adjusted multiple correlation coefficient, which represents the correlation level between the dependent variable and the independent variables. The calculation of adjusted R² considers the number of variables and can be used to compare goodness of fit of different regression models. Adjusted R² of the two regression equations are high, suggesting that the constructed regression models are reliable. The adjusted R² of equation (4) is higher than equation (2), implying a higher precision for the best-fit regression model. The significance test results on the regression equation suggest the significance of multiple regression equations ((F=173.5> F_{0.05}(2.883) for equation (2) and F=49.5> F_{0.05}(2.659) for equation (4)). Figures 6 and 7 show the distributions of the residuals in relation to the observed travel distance estimated by using equation (2) and (4). Both plots illustrates normality, constant variance and absence of trends in the residuals.

Figure 8 compares the predicted travel distances estimated by using equations (2) and (4) with the observed ones. It suggests that the predicted values of the samples are close to the observed ones. Where L exceeds 2000 m, the predicted travel distance calculated by using two models are lower than actual one, with relatively large residual error. The largest residual error appears in Wenjia gully rock avalanche, followed by Hongshi Gully, Niumian Gully and Donghekou rock avalanche. According to the field investigation, projected motion was experienced for these four rock avalanches with vertical drop of 260 m, 150 m, 60 m and 160 m respectively before they flowed along the channel downslope. Moreover, fluidization characteristics such as super-elevation near curve transitions can be found in the channel section of these four rock avalanches. These findings manifest the steep micro-geotopography will enlarge the mobility of rock avalanches as this kind of topography will lead the slide mass to undergo the projection, collision, fragmentation effects in the early motion stage which will facilitate



255 motion mode transformation from sliding to flowing. This transformation will enhance the motion
 256 mobility of rock avalanche to travel a much longer distance than predicted one.

257 4.3 Validation

258 The regression equations were tested using an independent sample validation data set (Table 4) of 8
 259 rock avalanches in the same area induced by three different kinds of triggers: 2008 M_s7.8 Wenchuan
 260 earthquake, 2013 M_s7.0 Lushan earthquake, and heavy rainfall. The volume of these samples ranged
 261 from 8.8×10^4 – $150 \times 10^4 \text{ m}^3$, and travel distance from 372–1372 m. The background parameters and the
 262 predicted values of each avalanche are listed in Table 4. The relative errors between the predicted
 263 values estimated by using equation (3) and observed values of the travel distance of the rock
 264 avalanches, $|L_{\text{predicted}} - L_{\text{observed}}| / L_{\text{observed}} \times 100\%$, are between -14.4% and 17.2%, while the
 265 relative errors are -44.0% and 17.9% for equation (4). On the whole, these two regression models
 266 achieved acceptable prediction accuracy for preliminary forecasting of travel distance of rock
 267 avalanches in rugged mountainous areas. The best-fit regression model appeared to provide greater
 268 precision than the alternative model. Regarding the influence of triggers on the travel distance of the
 269 channelized rock avalanches, those triggered by rainfall and the Lushan earthquake seemed to be more
 270 mobile. It is inferred that the former difference is due to the high water content in failed mass induced
 271 by rainfall. A possible reason why two rock avalanches triggered in the Lushan earthquake travelled
 272 farther may be because of structural weakening of slope rock mass in the 2008 Wenchuan earthquake
 273 in the study area.

274 5 Discussion

275 5.1 Prediction for travel distance of channelized rock avalanche

276 The results of our analysis of the data set, indicates that the mobility (travel distance) of channelized
 277 rock avalanche is positively correlated with landslide volume and total relief but negatively correlated
 278 with channel angle. It is inferred that the movement of channelized rock avalanche was strictly
 279 constrained by the local geomorphology. As Figure 5 shows, the travel distance of channelized rock
 280 avalanche would rapidly increase with volume of rock avalanche enlarged. Such a high correlation
 281 between landslide volume and travel distance implies that the travel distance of channelized rock
 282 avalanche is dominated by the spreading of the slide mass (Davies, 1982; Staron, 2009). The high



283 positive correlation between total relief and travel distance is for two reasons: **the larger the total relief**
 284 **is, the more kinetic energy the slide mass could obtained and the further distance could it travel.**

285 another contribution is the geometrical similarity of hillslope geomorphology in the study area (Legros,
 286 2002).

287 Regarding the **medium negative correlation** between travel distance and channel angle, it is inferred
 288 that when the slide mass rushed into the channel after the acceleration movement on the upper hillslope,
 289 it had relatively high velocity and extremely low frictional coefficient among the rock fragments, and
 290 the channel could not stop the rock avalanche **until it lost fragment flow discharge.** Hence, the travel
 291 distance of channelized rock avalanche would increase with the channel angle cut down given the same
 292 **flow discharge (landslide volume), relative stable flow velocity,** and similar flow capacity. However, it
 293 is still difficult to evaluate the flow capacity of the channels due to difficulty of quantifying its cross-
 294 section shape (width and depth of channels), resistance to the rock avalanche and even the shape
 295 changing induced by entrainment process of rock avalanche.

296 The residual analysis result demonstrates that the projection process in the early motion stage will
 297 significantly enlarge the travel distance of rock avalanches. The nature of this phenomenon is
 298 suggested to be involved with transformation of motion mode from sliding to flowing due to collision
 299 and fragmentation effects after the projection (Davies et al, 1999). Furthermore, the degree of
 300 fragmentation of failed mass should have remarkable influence on the travel distance of rock avalanche,
 301 and other factors changing the fragmentation degree should be further study, such as earthquake effect,
 302 geologic structure and rock type.

303 5.2 Conceptual model for transportation of channelized rock avalanche

304 The statistical results imply that the travel distance of channelized rock avalanche is highly correlated
 305 with landslide volume, total relief and channel angle. As the **total relief** and channel angle act as
 306 external factors for the motion of rock avalanche, it seems like it is in essence landslide volume that
 307 control the rock avalanche movement. Actually, a good fitting result between travel distance and
 308 landslide volume appears on our data set (Figure 4). So we propose a conceptual model for channelized
 309 rock avalanche transportation: An initial failed mass rushes into the channel with certain velocity after
 310 acceleration and fragmentation effects over the upper slope. Then the failed mass will “forget” the
 311 initial fall height and flow down in the channel like unsteady flow. The flow discharge (including



312 initial landslide volume and entrainment (initial volume) and the flow capacity of the channel control the
 313 travel distance of channelized rock avalanche without considering the motion mechanism.
 314 However, the flow capacity varies along the channel. Some local depression can store a mass of the
 315 moving rock debris, causing a lack of flow discharge for the downstream channel and a considerable
 316 decrease of travel distance. Taking Wenjia Gully rock avalanche for an example, almost a half of total
 317 volume of the landslide deposited on the beginning of the channel (red dash circle area in Figure 9),
 318 leading to that the distal deposition appeared in the channel instead of the valley. Thus assessing the
 319 flow capacity of the channel for rock avalanche motion will assist in future forecast of potential rock
 320 avalanche hazard in mountainous areas.

321 6 Conclusion

322 Channelized rock avalanche refers to a rock avalanche with a flow path confined between valley walls.
 323 Relevant Detailed data on thirty-eight channelized rock avalanches triggered by Wenchuan earthquake
 324 were collected by remote sensing, field investigation and literature review. The results of correlation
 325 and regression analysis revealed that the movement of channelized rock avalanches is dominated by
 326 spreading of the failed mass. Landslide volume (V), total relief (H) and channel angle (β) had
 327 predominant effects played a dominating role in the on travel distance of channelized rock avalanches.
 328 Stepwise multivariate regression was used to develop a nonlinear best-fit travel distance prediction
 329 model for the channelized rock avalanches. An alternative multivariate regression model was also built.
 330 The reliability of the two models was tested on by an independent validation dataset of 8 rock
 331 avalanches in the same area and produced good results, meeting the requirements for preliminary
 332 evaluation of travel distance for channelized rock avalanches in the Wenchuan earthquake area.

333 Acknowledgement

334 This work was supported by the Young Scientists Fund of the National Natural Science Foundation of
 335 China (Grant No. 41302241), the Fund for Creative Research Groups of China (Grant No. 41521002),
 336 the Fund for International Cooperation (NSFC-RCUK_NERC), Resilience to Earthquake-induced
 337 landslide risk in China (Grant No. 41661134010). The authors thank Dr. Mauri McSaveney for his
 338 constructive comments and editing the English the paper.

339



340 **References**

- 341 Davies, T. R., McSaveney, M. J., and Hodgson, K. A.: A fragmentation-spreading model for long-
 342 runout rock avalanches, *Canadian Geotechnical Journal*, 36, 1096-1110, 1999.
- 343 Fan, X., Rossiter, D. G., Westen, C. J., Xu, Q., and Görtin, T.: Empirical prediction of coseismic
 344 landslide dam formation, *Earth Surface Processes and Landforms*, 39, 1913-1926, 2014.
- 345 Finlay, P. J., Mostyn, G. R., and Fell, R.: Landslide risk assessment: prediction of travel distance,
 346 *Canadian Geotechnical Journal*, 36, 556-562, 1999.
- 347 Guo, D., Hamada, M., He, C., Wang, Y., and Zou, Y.: An empirical model for landslide travel distance
 348 prediction in Wenchuan earthquake area, *Landslides*, 11, 281-291, 2014.
- 349 Heim, A.: *Bergsturz und menschenleben* (No. 20), Fretz and Wasmuth, 1992.
- 350 Hungr, O., Evans, S. G., Bovis, M. J., and Hutchinson, J. N.: A review of the classification of
 351 landslides of the flow type, *Environmental and Engineering Geoscience*, 7, 221-238, 2001.
- 352 Hungr, O., and McDougall, S.: Two numerical models for landslide dynamic analysis, *Computers and*
 353 *Geosciences*, 35, 978-992, 2009.
- 354 Hungr, O., Leroueil, S., and Picarelli, L.: The Varnes classification of landslide types, an update,
 355 *Landslides*, 11, 167-194, 2014.
- 356 Hsü K J.: Catastrophic debris streams (sturzstroms) generated by rockfalls, *Geological Society of*
 357 *America Bulletin*, 86, 129-140, 1975.
- 358 Legros, F.: The mobility of long-runout landslides, *Engineering Geology*, 63, 301-331, 2002.
- 359 Lied, K., and Bakkehoi, S.: Empirical calculations of snow-avalanche run-out distance based on
 360 topographic parameters, *Journal of Glaciology*, 26, 165-177, 1980.
- 361 Lo, C. M., Lin, M. L., Tang, C. L., and Hu, J. C.: A kinematic model of the Hsiaolin landslide
 362 calibrated to the morphology of the landslide deposit. *Engineering Geology*, 123, 22-39, 2011.
- 363 Nicoletti, P. G., and Sorriso-Valvo, M.: Geomorphic controls of the shape and mobility of rock
 364 avalanches, *Geological Society of America Bulletin*, 103, 1365-1373, 1991.
- 365 Parker, R. N., Densmore, A. L., Rosser, N. J., De Michele, M., Li, Y., Huang, R., ... and Petley, D. N:
 366 Mass wasting triggered by the 2008 Wenchuan earthquake is greater than orogenic growth, *Nature*
 367 *Geoscience*, 4, 449-452, 2011.



- 368 Pastor, M., Haddad, B., Sorbino, G., Cuomo, S., and Drempetic, V.: A depth - integrated, coupled SPH
 369 model for flow - like landslides and related phenomena, *International Journal for numerical and*
 370 *analytical methods in geomechanics*, 33, 143-172, 2009.
- 371 Qi, S., Xu, Q., Zhang, B., Zhou, Y., Lan, H., and Li, L.: Source characteristics of long runout rock
 372 avalanches triggered by the 2008 Wenchuan earthquake, China, *Journal of Asian Earth Sciences*, 40,
 373 896-906, 2011.
- 374 Sassa, K.: Geotechnical model for the motion of landslides, In: AA Balkema (ed.) *Proceedings of the*
 375 *5th International Symposium on Landslide*, Rotterdam, 37-55, 1988.
- 376 Scheidegger, A. E.: On the prediction of the reach and velocity of catastrophic landslides, *Rock*
 377 *Mechanics and Rock Engineering*, 5, 231-236, 1973.
- 378 Staron, L., and Lajeunesse, E.: Understanding how volume affects the mobility of dry debris flows,
 379 *Geophysical Research Letters*, 36, 2009.
- 380 Van Westen, C. J., Van Asch, T. W., and Soeters, R.: Landslide hazard and risk zonation—why is it
 381 still so difficult?, *Bulletin of Engineering geology and the Environment*, 65, 167-184, 2006.
- 382 Xu, Q., Pei, X. J., and Huang, R. Q.: Large-scale landslides induced by the Wenchuan earthquake.
 383 *Science*, Beijing, 2009 (In Chinese).
- 384 Yu, H., Wang, D., Yang, Y., Xie, Q., Jiang, W., and Zhou, B.: The preliminary analysis of strong
 385 ground motion records from the M_s 8.0 Wenchuan Earthquake, *Journal of Earthquake Engineering*
 386 *and Engineering Vibration*, 1, 000, 2009.
- 387 Zhang, M., and Yin, Y.: Dynamics, mobility-controlling factors and transport mechanisms of rapid
 388 long-runout rock avalanches in China, *Engineering Geology*, 167, 37-58, 2013.
- 389
 390

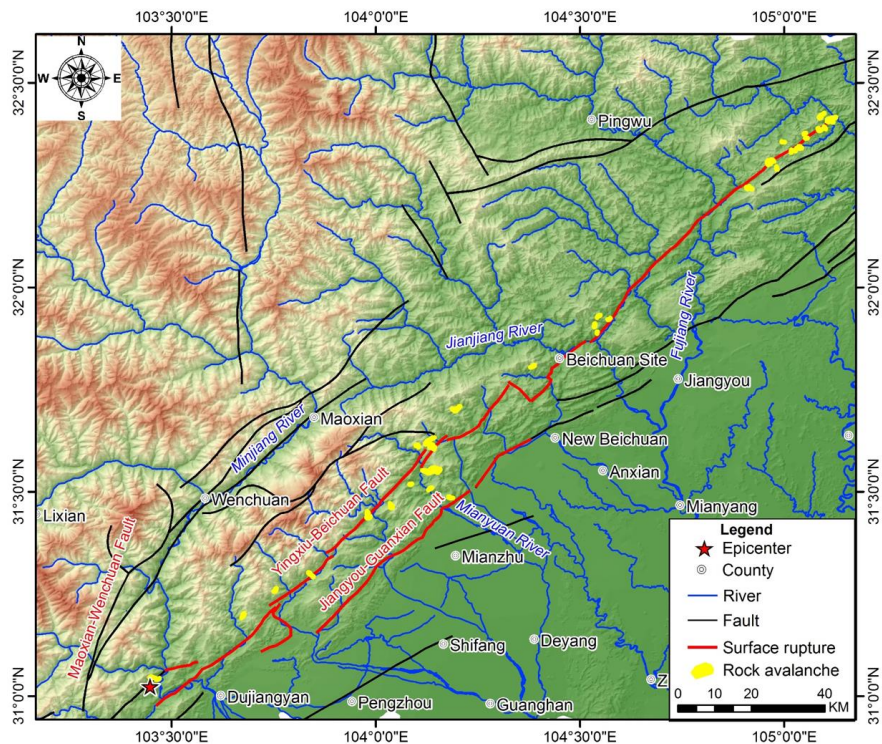
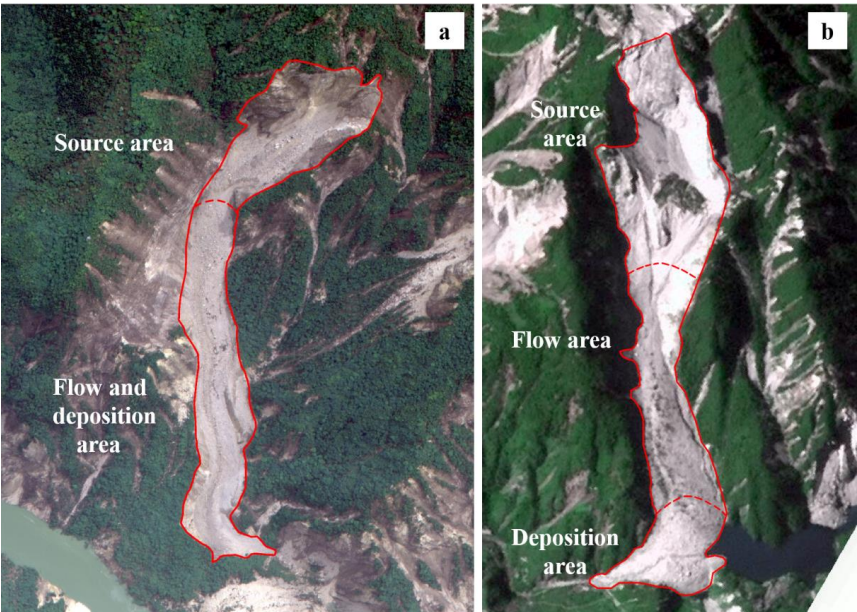
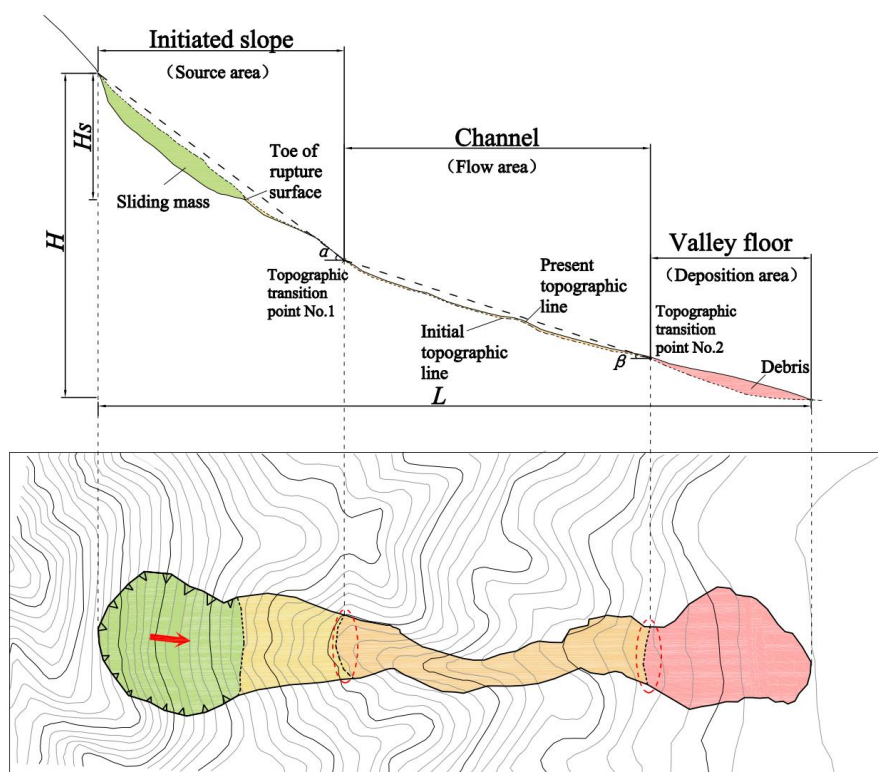


Figure 1: Distribution map of large rock avalanches triggered by the Wenchuan earthquake.





395 Figure 2: Remote-sensing images of two channelized rock avalanches triggered by the Wenchuan
 396 earthquake. a is Changtan rock avalanche (No.21 in table 1); b is Laoyingyan rock avalanche, which is
 397 river-blocked.



398
 399 Figure 3: Sketch map of a channelized rock avalanche defining geometric parameters. The red-dashed
 400 ellipse indicates the topographic transition dividing the initiated slope, channel and valley floor. The red
 401 arrow represents sliding direction of source mass.

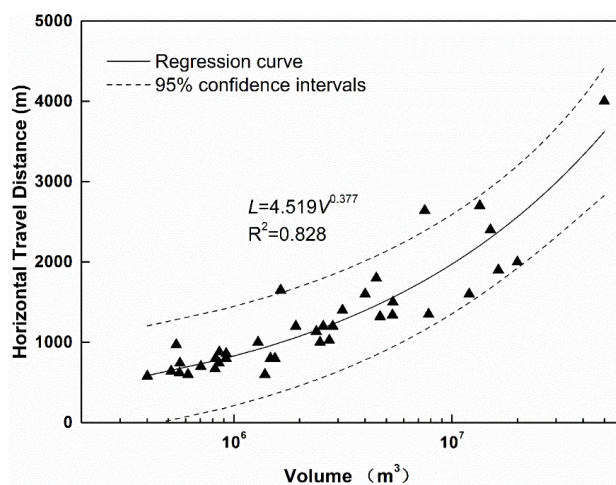


Figure 4: Relationship between horizontal travel distance and volume of channelized rock avalanches.

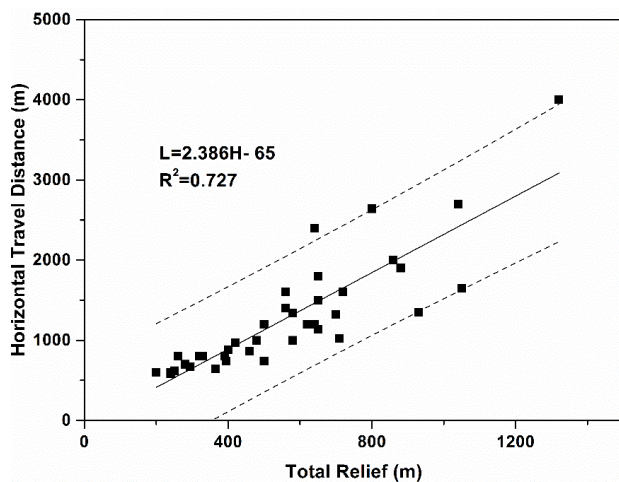


Figure 5: Relationship between horizontal travel distance and total relief of channelized rock avalanche.

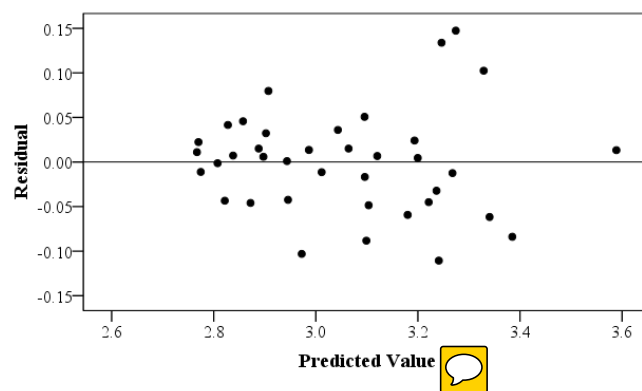


Figure 6: Residual plot for equation (2).

404

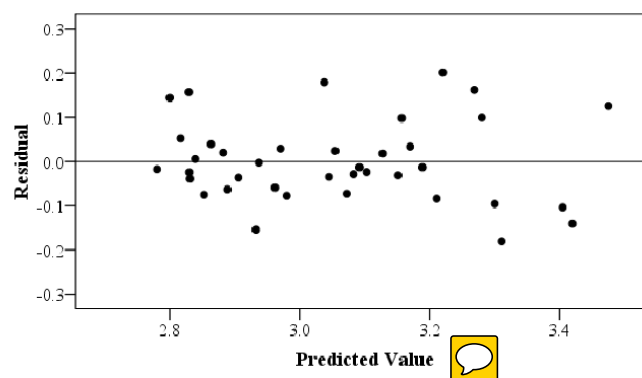


Figure 7: Residual plot for equation (4).

405

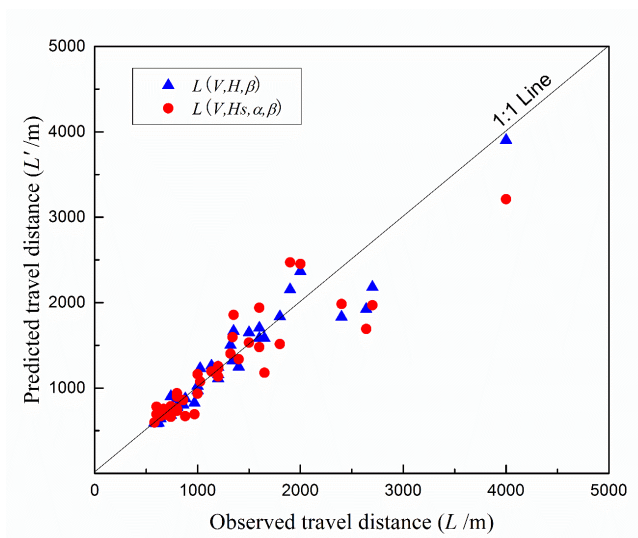
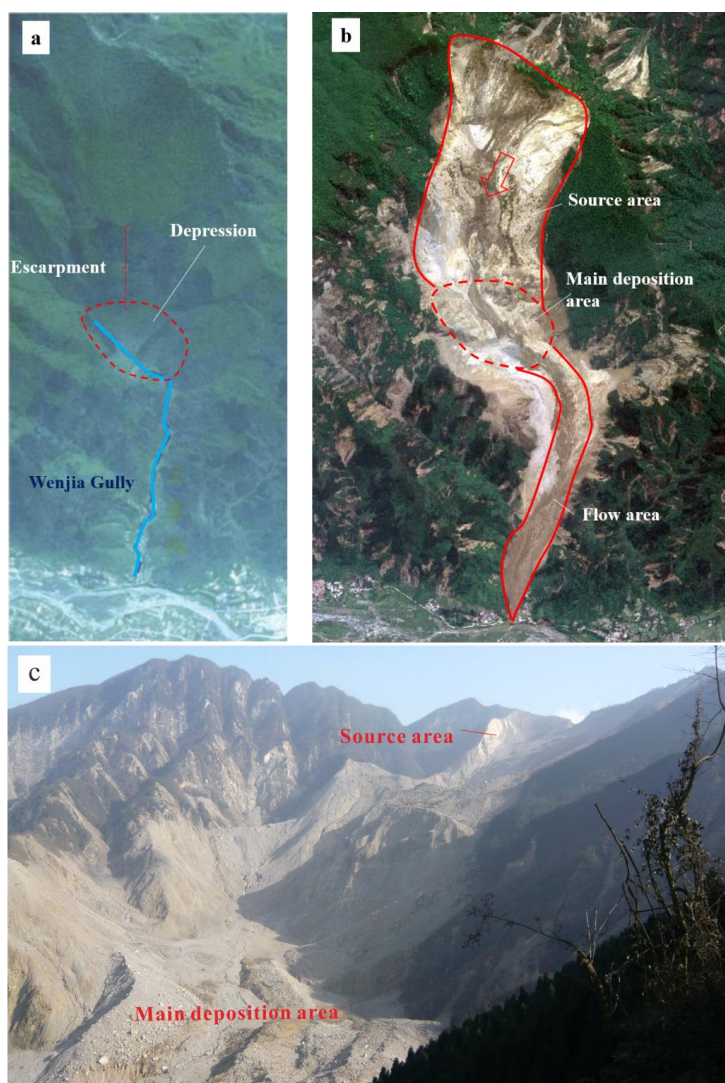


Figure 8: The comparison between observed and predicted travel distance for the two multivariate regression models.



406

407 **Figure 9: Sketch map of flow capacity of channel affecting on the travel distance of Wenjia Gully**
 408 **channelized rock avalanche: (a) before the earthquake, (b) after the earthquake, (c) photo taken on**
 409 **deposition platform after the earthquake. The red arrow show the sliding direction of source mass. The red**
 410 **dotted line in figure.9(a) indicates the original depression on the travel path of the rock avalanche, in where**
 411 **debris deposition of about 30 million m³ was stored after the earthquake (shown in figure.9(b)), and more**
 412 **detailed information is shown in the figure.9(c).**



Table 1: Data of various factors for establishment of prediction model of rock avalanche travel distance.

Code	Landslide name	Longitude, (°E)	Latitude, (°N)	Landslide area, A (m^2)	Landslide volume, V (m^3)	Source area height, H_s (m)	Slope angle, α (°)	Channel angle, β (°)	Total relief, H (m)	Travel distance, L (m)	Reference
1	Wenjia Gully	104.140	31.552	3000566	50000000	440	26	7	1320	4000	Xu et al., 2009
2	Shuimo Gully	103.981	31.442	915608	19960000	490	35	10	860	2000	
3	Dawuji	104.196	31.702	792190	16330000	540	29	13	880	1900	
4	Donghekou	105.113	32.410	1283627	15000000	240	25	11	640	2400	Xu et al., 2009
5	Hongshigou	104.130	31.624	687520	13410000	290	37	17	1040	2700	
6	Woqian	104.964	32.308	695672	12000000	330	30	10	560	1600	Xu et al., 2009
7	Xiaoliashan	104.038	31.465	465899	7810000	480	48	24	930	1350	
8	Niumian Gully	103.456	31.044	527700	7500000	320	32	13	800	2640	Xu et al., 2009
9	Liqi Gully	105.207	32.169	355113	5360000	360	37	12	650	1500	
10	Caocaoping	104.139	31.607	354046	5340000	345	31	17	580	1340	
11	Huoshi Gully	104.134	31.616	322155	4680000	270	38	17	700	1320	
12	Shibangou	105.090	32.419	496983	4500000	450	34	9	650	1800	Xu et al., 2009
13	Xiejadianzi	103.841	31.298	294256	4000000	400	34	15	720	1600	Xu et al., 2009
14	Dashui Gully	103.675	31.199	241874	3150000	320	30	17	560	1400	
15	Changping	103.754	31.259	224645	2840000	290	37	16	500	1200	
16	Xiaomuling	104.102	31.613	218704	2740000	175	45	26	710	1025	
17	Baishuling	104.385	31.807	208968	2570000	335	36	20	620	1200	
18	Dawan	104.536	31.907	203959	2480000	220	28	20	480	1000	
19	Xiaoliashan	104.182	31.486	198165	2385499	340	44	20	650	1135	
20	Shicouzi	104.918	32.243	169540	1920000	260	30	26	640	1200	



21	Changtan	104.133	31.508	151094	1640000	400	33	25	1050	1650
22	Hongmagong	104.962	32.301	144683	1540000	195	30	14	330	800
23	Baiguocun	105.088	32.385	139800	1470000	165	26	12	260	800
24	Qinglongcun	105.036	32.342	134079	1390000	90	21	11	200	600
25	Pengjiashan	104.546	31.930	127156	1290000	200	33	28	580	1000
26	Longwancun	104.571	31.922	99821	920000	205	31	28	460	860
27	Zhangzhengbo	105.017	32.333	99726	920000	125	29	15	320	800
28	Dujiayan	105.028	32.336	94769	860000	100	33	17	400	880
29	Madiping	104.996	32.355	94632	860000	140	27	31	395	740
30	Yandiaowo	105.099	32.391	92128	820000	145	30	26	390	800
31	Chuangzi Gully	104.085	31.518	91717	820000	185	35	15	295	670
32	Zhaoliashan	105.041	32.342	82329	700000	115	22	16	280	700
33	Weiziping	105.083	32.387	74661	620000	135	22	18	240	600
34	Maochongshan 2	104.908	32.243	70251	570000	160	38	22	500	740
35	Waqianshan	105.049	32.376	70007	560000	135	24	18	250	620
36	Muhongping	104.982	32.291	68288	540000	175	28	20	420	970
37	Dapingshang	104.542	31.889	65700	520000	160	34	29	365	640
38	Liushuping 2	105.054	32.365	54810	400000	150	29	16	240	580



Table 2: Correlation coefficients of continuous variables listed in Table 1.

	A	V	H	Hs	α	β	L
A	1.000	0.982	0.674	0.521	-0.119	-0.524	0.877
V	—	1.000	0.713	0.560	-0.055	-0.492	0.866
H	—	—	1.000	0.801	0.429	-0.130	0.857
Hs	—	—	—	1.000	0.399	-0.323	0.675
α	—	—	—	—	1.000	0.264	0.082
β	—	—	—	—	—	1.000	-0.467
L	—	—	—	—	—	—	1.000

Note: The number in Italics indicates the two variables are not significantly correlated

Table 3: The regression coefficients and results of significance tests of two multivariate regression models.

Equations	Coefficients*	Intercept	Coefficient of log(V)	Coefficient of log(H)	Coefficient of log(tan β)	Coefficient of log(Hs)	Coefficient of log(tan β)	Adjusted R ²	F-stat	F _{0.05}
Best-fit regression equation	LCI	0.175	-0.013	0.521	-0.548	—	—	—	—	—
	Mean	0.420	0.079	0.718	-0.365	—	—	0.933	173.5	2.883
	UCI	0.665	0.171	0.914	-0.182	—	—	—	—	—
Alternative regression equation	LCI	0.110	0.199	—	-0.165	-0.002	-0.464	—	—	—
	Mean	0.561	0.303	—	0.072	0.244	-0.115	0.840	49.5	2.659
	UCI	1.012	0.407	—	0.308	0.489	0.233	—	—	—

5 Note: “Coefficients” of each variable has three kinds: LCI is lower bound of the coefficients with 95% confidence; Mean is the mean value of the coefficients; UCI is upper bound of the coefficients with 95% confidence;

Table 4: Background parameters and predicted values of 8 rock avalanches in the same area used for validation

Landslide name	Longitude	Latitude	Triggers*	V /10 ⁴ m ³	α /°	B /°	Hs /m	H /m	L /m	L' (3)** /m	Error /%	L' (4)*** /m	Error /%
Pianqiaozi	104.370	31.822	WCEQ	8.8	35	19	153	205	372	436	17.2	373	0.3
Yangjiayan	104.328	31.755	WCEQ	25.4	41	23	164	304	518	583	12.5	518	0.1
Shanshulin	103.508	31.181	WCEQ	27.9	34	25	340	433	715	731	2.3	660	-7.6
Fuyangou	103.501	31.422	WCEQ	71.9	38	28	385	530	763	869	13.8	900	17.9



Dayanbeng1	102.762	30.179	LSEQ	100	53	10	254	424	1267	1136	-10.3	781	-38.4
Dayanbeng2	102.761	30.178	LSEQ	110	50	8	237	407	1372	1208	-12.0	787	-42.6
Ermanshan	102.739	29.322	RF	100	33	15	148	635	1370	1303	-4.9	767	-44.0
Wulipo	103.567	30.919	RF	150	30	10	135	377	1260	1078	-14.4	833	-33.9

Note: “Triggers” is the triggering condition of rock avalanches: “WCEQ” represents the 2008 Wenchuan Ms7.8 earthquake;
“LSEQ” represents the 2013 Lushan Ms7.0 earthquake; “RF” represents the rock avalanche was induced by heavy rainfall.
 $L'_{(3)}$, $L'_{(4)}$ indicates the predicted travel distance estimated by using equation (3) and (4) respectively.